Microscopical heat stress investigations under application of quantum dots

Cathrin Dressler
Charité Universitätsmedizin in Berlin
Institut für Medizinische Physik und Lasermedizin
Campus Benjamin Franklin
Fabeckstrasse 60-62
D-14195 Berlin
Germany
and
Laser und Medizin Technologie GmbH, Berlin
Fabeckstrasse 60-62
D-14195 Berlin
Germany
E-mail: c.dressler@lmtb.de

Olaf Minet
Jürgen Beuthan
Vladimir Novkov
Gerhard Müller
Charité Universitätsmedizin in Berlin
Institut für Medizinische Physik und Lasermedizin
Campus Benjamin Franklin
Fabeckstrasse 60-62
D-14195 Berlin
Germany

Abstract. Heat stress responses are analyzed in cancer cells by applying different microscopy techniques for targeting various fluorescently labeled or native structures. Thermotreatments are performed at 40, 45, 50, and 56 °C, respectively, for 30 min each, while controls were kept at 37 °C. Actin cytoskeletons labeled with Alexa Fluor® 488-conjugated phalloidin are imaged by wide-field fluorescence microscopy (WFFM). Structural plasma membrane stabilities are labeled with fluorescent quantum dots and analyzed by laser scanning microscopy (LSM). High-resolution atomic force microscopy (AFM) and scanning electron microscopy (SEM) are used to study morphological features and surface structures. Fluorescence images reveal F-actin to be a comparatively thermolabile cell component showing distinctive alteration after heat treatment at 40 °C. Destabilization of actin cytoskeletons proceed with increasing stress temperatures. Active reorganization of plasma membranes coincidental to heat-induced shrinkage and rounding of cell shapes, and loosening of monolayered tissue are observed after treatment at 45 or 50 °C. Active stress response is inhibited by stress at 56 °C, because actin cytoskeletons as well as plasma membranes are destroyed, resulting in necrotic cell phenotypes. Comparing data measured with the same microscopic technique and comparing the different datasets with each other reveal that heat stress response in MX1 cells results from the overlap of different heat-induced subcellular defects. [DOI: 10.1117/1.2001674]

Keywords: heat stress response; breast cancer cells; quantum dots; wide-field fluorescence microscopy; laser scanning microscopy; atomic force microscopy.

Paper SS04205R received Oct. 29, 2004; revised manuscript received Jan. 31, 2005; accepted for publication Feb. 22, 2005; published online Aug. 15, 2005.

1 Introduction

Cells exposed to heat stress undergo multiple molecular alterations, including synthesis and augmented production of heat-shock proteins, protein misfolding or damaging, and energy depletion. These initial events possibly trigger complex interactions of metabolic mechanisms and signal transductions that determine cellular stress responses. Depending on the heat stress dose, comprising temperature and exposure time, the cell species, and the tissue architecture and environment, the stress responses lead to cell survival, apoptosis, or necrosis. In this context, heat stress represents a large array of various physical, biochemical, toxicological, and environmental stress factors.[1–3] In the field of clinical cancer therapy, two major groups comprise thermotherapy: laser-induced thermotherapy inducing local temperatures between 60 and 100 °C,[4,5] and hyperthermia working with temperatures below 45 °C.[6] Combined modality treatments such as hyperthermia-assisted radiotherapy and/or chemotherapy are under intensive investigation.[7,8] A new thermotherapeutic approach has been published by Jordan et al. that suggests injection of magnetic nanoparticles into the tumor, followed by application of alternating current magnetic fields, inducing a temperature elevation in the particle-loaded tissue.[9]

Dosimetry remains a critical factor in thermotherapy, since therapy responses might vary among different tissue species, tissue volumina, tissue entities, and tissue environments.[10] With regard to dosimetry in medical thermotherapeutic applications, adequate knowledge about cellular and subcellular reactions to thermal stress conditions is essential. The molecular genetics of heat stress responses already have been studied extensively and reviewed by Takayama, Reed, and Homma,[11] and Moggs and Orphanides.[12] Representative examples of cellular heat-induced phenotypes using an Arrhenius-based approach have been studied *in vitro* by Dewhirst et al.[10] and *in vivo* by Minet and Beuthan.[13]

In the present study, we investigated the stress responses of breast cancer cells MX1 under hyperthermal (40 °C) and heat stress (45, 50, or 56 °C) conditions. Several different subcellular sites were targeted to characterize their impact on heat-induced phenomena.

Address all correspondence to Cathrin Dressler, Laser-Medizin-Technologie Berlin, Fabeckstrasse 60–62, Berlin 14195 Germany. Tel: *49–30–8449–326; Fax:*49–30–8449–23399; E-mail: c.dressler@lmtb.de

1083-3668/2005/10(4)/041209/9/$22.00 © 2005 SPIE

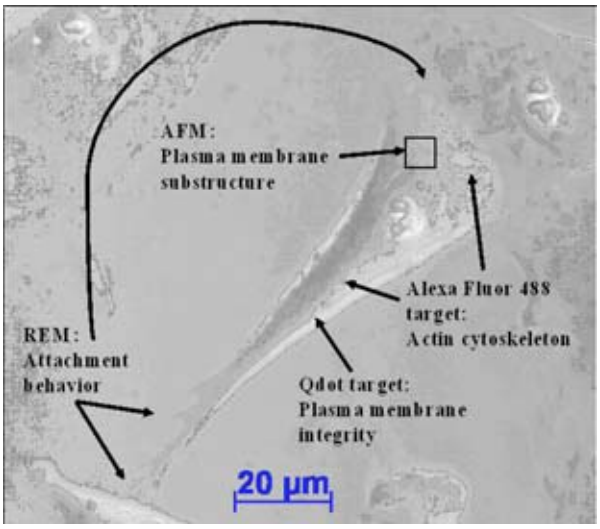

Fig. 1 Schematic view of a MX1 breast cancer cell showing the investigation targets of this study.

The most versatile approach for probing stress-induced effects in cells is fluorescence microscopy, as it is one of the best established standard techniques in biomedical analytics and diagnostics. Fluorescence detection of specific structures and functions in cells is supported by an enormous diversity of commercial fluorescent probes and biosensors mainly tailored for specific targets as well as spectral properties.[14,15] Many organic fluorescent dyes, immunoconjugates, and GFP-based biosensors have been routinely used for imaging cells; recently, several bioactive nanoparticles have entered the field of experimental bioanalytics. Most interesting among those are magneto/optical nanoparticles,[16] as well as luminescent quantum dots (Qdots).[17,18] Various surface modifications and conjugation strategies have been developed for improving stabilities and bioactivities of Qdots without altering their unique spectral properties resulting from semiconductor effects.[19–22] The bright and narrow-banded fluorescence emissions combined with broad excitation ranges and high absorptions of Qdots especially are relevant features concerning bioanalytical applications. Qdot fluorescence colors in the visible spectrum depend on the semiconductor material and mainly on particle diameters roughly ranging from 2 to 6 nm. The broad spectral variability of Qdots also makes them very interesting tools in many kinds of multiplexed labeling strategies.[23,24]

As shown previously, MX1 cell viability did not decrease after hyperthermal treatment at 40 or 42 °C, but after heat stress at temperatures of 45, 50, or 56 °C, cell viabilities had drastically diminished.[25] In this study the metabolic data were supplemented by molecular fluorescence imaging and high-resolution structural imaging. The following targets were compared using a defined heat stress protocol: plasma membrane, actin cytoskeleton, and attachment filaments, as shown in Fig. 1. The microscopic techniques listed in Table 1 were used depending on the particular target.

It was shown by wide-field fluorescence microscopy (WFFM) and laser scanning microscopy (LSM), respectively, that the actin cytoskeleton in MX1 cells already responded at comparatively mild stress conditions of 40 °C (30 min), while cell morphologies and plasma membrane integrities were not affected. Under increased stress temperatures, rearrangements of actin filaments were enhanced and accompanied by striking changes of cell shapes. Inline with cytoskeletal destabilization, the surface substructures increase with temperatures as visualized by atomic force microscopy (AFM). On severe heat stress at 56 °C (30 min), actin cytoskeletons as well as plasma membranes were completely destroyed, resulting in cell necrosis. Treatment at 50 °C for 30 min was not sufficient for induction of necrosis, but the

Table 1 Microscopes and measurement configurations used for imaging various targets of heat-induced stress response in MX1 cancer cells. LP is a long-pass filter, BP is a bandpass filter, bw is black and white, and C is for color.

Microscope system	Measurement configuration	Investigation target
DSM950 (Carl Zeiss, Germany)	• Accelerating voltage: 5 kV • Working distance: 6 to 9 mm	Cell morphology, surface structures, cell-cell and cell-substrate contacts
Axioplan 2 (Carl Zeiss, Germany)	• Excitation range: BP 470±20 nm • Detection range: LP>520 nm • Signal digital camera: AxioCam MRc	Alexa Fluor® 488 fluorescence at phalloidin-labeled F-actin
LSM 410 invert (Carl Zeiss, Germany)	• Laser wavelengths: 568 and 488 nm • Detection range: LP>590 nm • Signal detector: photomultiplier • Digital camera: Sony CCD-IRIS Hi-Resolution (bw) • Integration time: 16 s/scan	Qdot™ 605 fluorescence at concanavalin A-labeled structures
easyScan DFM (NanoSurf, Switzerland)	• Operation mode: dynamic force • Operating frequency: 156 to 160 kHz • Integration time: 256 to 410 s/scan • Spring constant: 0.20 N/m • Cantilever type: reflex-coated n^*-silicon pointprobes (NanoWorld AG, Switzerland) • Free operating amplitude: 0.5 V • Vibration damping: TS-150 (Schaefer Technology GmbH, Germany)	Surface roughness of cells

cells exhibited altered morphological features as a result of active stress response, as shown by fluorescence microscopy and scanning electron microscopy (SEM).

2 Material and Methods

All chemicals were purchased from Sigma-Aldrich Chemie GmbH, Germany, unless stated otherwise.

2.1 *Cell Cultivation*

Human undifferentiated breast cancer cells of the species MX1 (Deutsches Krebsforschungszentrum, Germany) were cultivated in RPMI 1640 medium supplemented with 20–mM HEPES (N-2-hydroxyethylpiperazine-N-2-ethanesulfonic acid) buffer, 5% (v/v) heat inactivated fetal calf serum, and 1% (v/v) antibiotic-antimycotic solution (100–U/mL penicillin, 100-μg/mL streptomycin, and 0.25-g/mL amphotericin B; GIBCO™ Invitrogen GmbH, Germany) at 37 °C in a humidified atmosphere. Monolayers were dissociated with 0.05% trypsin-0.02% EDTA. All culture medium components and solutions were purchased from Biochrom KG seromed®, Germany, if not stated otherwise. Experimental cells were grown in chambered glass slides with four chambers per slide (NUNC GmbH and Company KG, Germany) or on coverslips (SEM) until subconfluent cell densities were achieved.

2.2 *Heat Stressing*

Heat treatments were performed in a temperature-regulated water bath at 40, 45, 50, or 56 °C for 30 min each. Cells were rinsed twice in cold phosphate buffered saline (PBS) immediately after heat stress and submitted for further processing as described in the following sections.

2.3 *Preparation of Unlabeled Cells*

Prior to AFM measurements, cellular structures were stabilized by fixation in 2.5% glutaraldehyde-PBS solution for $\geqslant$1 h at 4 °C. SEM investigations required cells grown on coverslips to be fixated in 2% glutaraldehyde-1% cacodylate buffer (*p*H 7.3) solution for 10 min, followed by dehydration in graded ethyl alcohol (50 to 100%). Dehydrated cells then were treated twice with hexadimethydisilazane for 3 min. After desiccation, SEM samples were sputtered with gold (150 s, 10-nm layer thickness).

2.4 *Fluorescent Dye Labeling*

Labeling of cytoskeletal F-actin with Alexa Fluor® 488 -conjugated phalloidin was performed according to the manufacturer's (Molecular Probes, Netherlands) recommendations. Since phallotoxins usually are cell impermeable, labeling of cells with Alexa 488-phalloidin conjugate (approximately 0.3 μM) was conducted under permeabilizing and fixating conditions: 20 min in 100-μg/mL lysopalmitoylphosphatidyl-choline and 3.7% formaldehyde solution at 4 °C (Sigma-Aldrich Chemie GmbH, Germany).[26]

2.5 *Quantum Dot Labeling*

Streptavidin-conjugated Qdot™ 605 (Quantum Dot Corporation, USA) nanocrystals were used to label plasma membranes via biotinylated concanavalin A (ConA, Molecular Probes, Netherlands). Internal biotin of cells was first blocked by treatment with 50-μg/mL Avidin (Sigma Aldrich Chemicals, Germany) in PBS 30 min at 37 °C before 250-μg/mL ConA-biotin in PBS was applied (30 min, 37 °C). The Qdot-streptavidin conjugate was used to label cell-bound ConA mediated by biotin:streptavidin bridging. Qdot-conjugate stock solution was diluted 1:10 in incubation buffer supplied by the manufacturer 20 min prior to application. The final concentration of 0.1 μM was obtained by mixing equal volumes of PBS and Qdot solution. After 30-min incubation, the cells were rinsed three times and micrographed in PBS. Every step was incubated for 30 min at 37 °C and stopped by rinsing the cells carefully in cold PBS. This labeling protocol was mainly based on the manufacturer's recommendations,[27] with alterations mentioned earlier.

2.6 *Microscope Systems*

For fluorescence imaging of Qdot-labeled cells, a laser-scan microscope LSM 410 inverse (Carl Zeiss, Germany) was used. Alexa-488 fluorescence of F-actin was imaged with an Axioplan 2 (Carl Zeiss, Germany). Scanning electron microscopy was performed with a DSM950 (Carl Zeiss, Germany). A mobile atomic-force microscope easyScan DFM (Nanosurf, Switzerland) was applied in the dynamic-force mode for near-field investigations. All microscope systems and measurement configurations used in this study are listed in Table 1.

3 Results

3.1 *SEM Imaging of Cell Morphologies, Cell-Cell, and Cell-Substrate Adhesion Behavior*

SEM investigations were done to gain an overview of morphological responses of MX1 cells to heat treatments. Also, the intercellular contact behavior and cell-substrate adhesion were the subject of the SEM experiment. As expected, control cells (37 °C) and cells stressed at 40 °C exhibited tissue-specific growth conformations and cell morphologies with structural integrities [Figs. 2(a) and 2(b)]. Cells were well spread on the glass substrate and adherently grown with polygonal orientations, distinct intercellular contacts, and extended intermediate filaments. Cells in the 40 °C-stress group were slightly flattened and cell surfaces appeared smoother than in the control group. When stressing was performed at 45 or 50 °C, [Figs. 2(c) and 2(d)] cells became smaller and more spheroidal shaped compared with control cells [Fig. 2(a)]. Consequently, the tissue was clearly dispersed resulting from active cellular stress reactions during heat treatment. This effect was more pronounced in the 50 °C-stress group than in the 45 °C-stress group. The spheroid cell shapes seen in Fig. 2(c) were not observed in Fig. 2(d), indicating that cells already were in a collapsed state after heat stress at 50 °C. 30 min of thermal treatment at 56 °C also induced distinctive ruptures in the plasma membranes, as evidenced by the collapse of cells. These cell and tissue morphological features imaged by SEM were generally observed independent of the microscope technique or sample preparation method applied.

3.2 *Fluorescence Detection of F-Actin Cytoskeletons*

Heat-induced reactions of F-actin cytoskeletons in MX1 cells were imaged by green fluorescence of Alexa Fluor® 488 con-

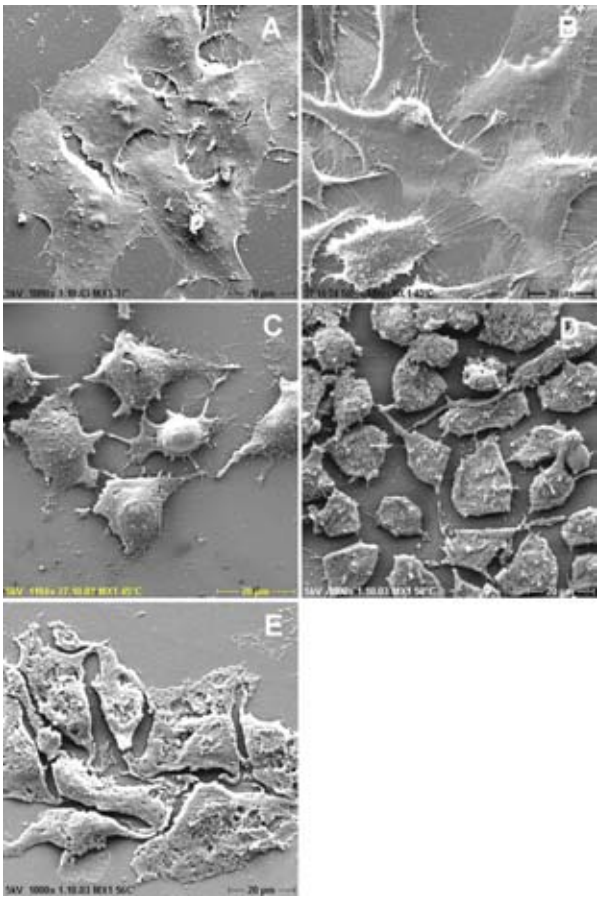

Fig. 2 Scanning electron microscopy of MX1 cells treated at various heat stress conditions as indicated: (a) control cells, (b) cells stressed at 40 °C, (c) cells stressed at 45 °C, (d) cells stressed at 50 °C, and (e) cells stressed at 56 °C (30 min each). Details of the measurement setup are given in Table 1.

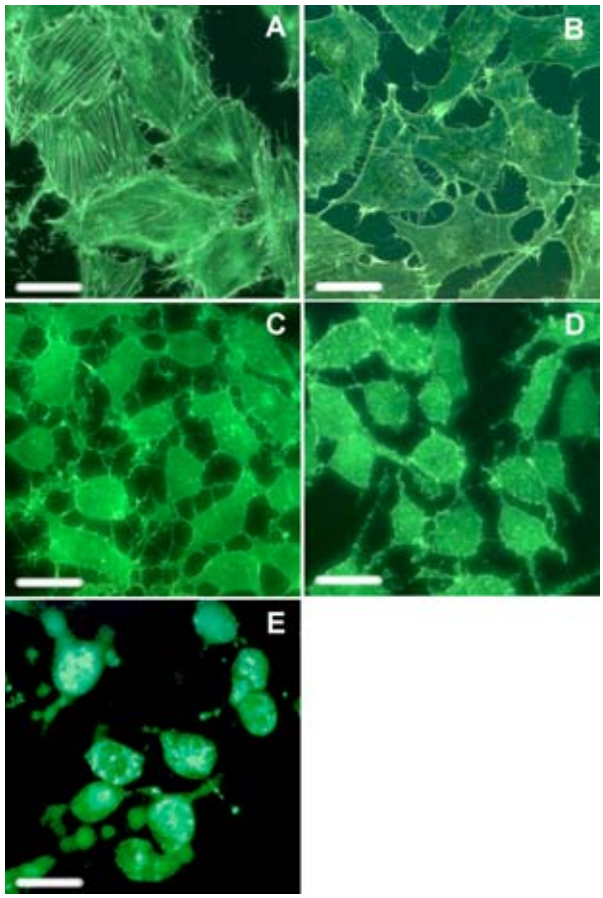

Fig. 3 Fluorescence imaging of cytoskeletal F-actin in MX1 cells treated at various heat stress conditions as indicated. The fluorescence label is Alexa Fluor® 488 conjugated to actin-bound phalloidin (Molecular Probes, Netherlands): (a) control cells, (b) cells stressed at 40 °C, (c) cells stressed at 45 °C, (d) cells stressed at 50 °C, and (e) cells stressed at 56 °C (30 min each). Excitation range: BP 470±20 nm, detection range: LP>520 nm. Details of the measurement setup are given in Table 1. The scale bar is 20 μm.

jugated to F-actin-bound phalloidin. Under increasing heat stress conditions, the F-actin components exhibited drastic structural alterations, as shown in Fig. 3. In control cells [Fig. 3(a)], actin exhibited long filamentous structures forming intact networks within the cell bodies. Intact contacts with F-actin in plasma membranes were stabilizing the cell morphologies and intercellular connections. After treatment at 40 °C, F-actin networks already were destabilized, as evidenced by diminished filamentous structures; however, plasma membranes and intercellular contacts had not yet been affected. Corresponding with the SEM image [Fig. 2(c)], heat stress at 45 °C induced loosening of tissue as well as advanced disintegration of cytoskeletons, leading to shrinkage and rounding of cells. F-actin structures in cells stressed at 50 °C contained even more defects, where it was observed that the actin particles clustered in the cytoplasm and at membranes. A total breakdown of tissue cohesion and cytoskeletal structures resulted from heat stress at 56 °C.

3.3 *Fluorescence Detection of Qdot-Labeled Plasma Membranes*

In control cells and 40 °C-stressed cells, Qdot fluorescence was localized at the superficial areas of plasma membranes and intercellular connections [Figs. 4(a) and 4(b)]. Fluorescence intensities were irregularly distributed along the plasma membranes, indicating variant compositions and frequencies of carbohydrate residues in the glycocalix. The intensities were higher in Fig. 4(b) than in Fig. 4(a) because of enhanced ConA binding. After stressing at 45 or 50 °C [Figs. 4(c) and 4(d)], cells again were smaller and rounder than in the control group [Fig. 4(a)]. The 3-D intensity profiles exhibited more regular fluorescence distributions than under milder stress conditions at 40 °C. Qdot fluorescence at the same time was also detected at the cytoplasmic leaflets of plasma membranes, supporting the presumption that plasma membranes were reorganized, permitting Qdot conjugates to accumulate inside plasma membranes. Nuclei in the cells of the 50 °C-stress group were intact to the extent that they did not exhibit fluorescence accumulation. Cells were severely damaged at 56 °C, presenting necrotic phenotypes because the structural integrities of plasma membranes and nuclear membranes were destroyed. Now Qdot fluorescence accumulated inside the cells [Fig. 4(e)].

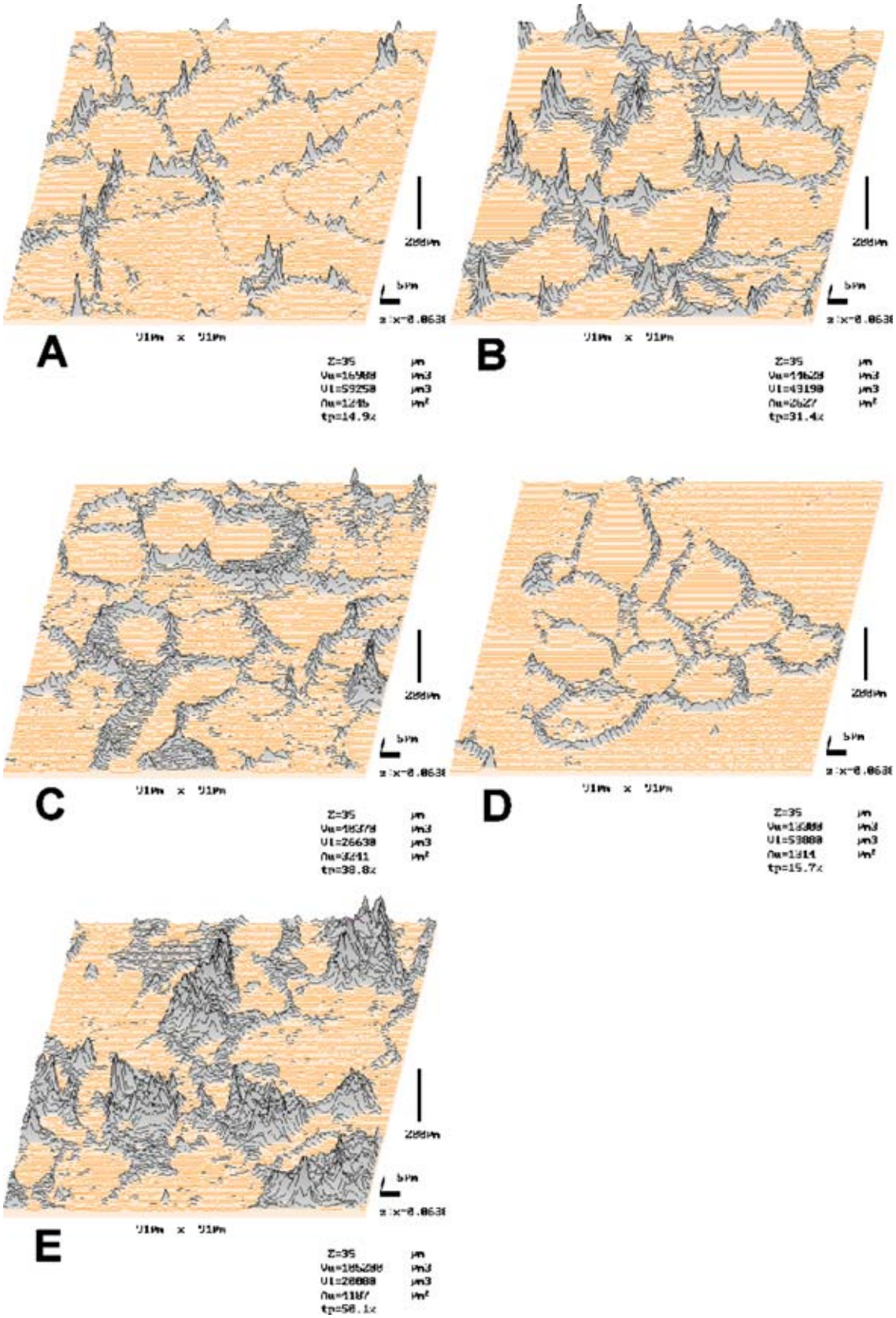

Fig. 4 Fluorescence imaging of plasma membranes in MX1 cells labeled with Qdots (Quantum Dot Corporation, USA). The fluorescence distributions are imaged as 3-D signal intensity profiles: (a) control cells, (b) cells stressed at 40 °C, (c) cells stressed at 45 °C, (d) cells stressed at 50 °C, and (e) cells stressed at 56 °C (30 min each). Details of the measurement setup are given in Table 1.

3.4 *AFM Imaging of Plasma Membrane Topographies*

AFM measurements focusing on the area roughness of cell surfaces were performed in dynamic force operation mode. The membrane surfaces of control cells were more or less regularly undulated without showing indentation or incisions [Fig. 5(a)]. After treatment at 40 °C, the topography in Fig. 5(b) exhibited a more jagged and less regular structure than the control cell. The surface roughness was further increased after 45 °C heat stress, since globular protruding substructures led to spot-like cavities, as shown in Fig. 5(c). This effect was enhanced after treating cells at 50 °C [Fig. 5(d)], where the cavities were more stretched like clefts. Heat shock at 56 °C actually did not change the surface structures of the cells [Fig. 5(e)] compared to the 50 °C-treated cells, but the sizes of cavities were increased, appearing like holes. The area roughness of the cell shown in Fig. 5(e) was increased. The development of this temperature-dependent effect is represented by a quantitative evaluation of the mean surface area roughness (S_a) illustrated in Fig. 6. S_a values were measured for the topographies shown in Fig. 5 using the following equation:[28,29]

$$S_a = \frac{1}{MN} \sum_{k=0}^{M-1} \sum_{l=0}^{N-1} |z(x_k, y_l)|.$$

4 Discussion

Heat as the classical form of stress factor induces manifold molecular changes in animal cells, including the synthesis of heat-shock proteins, leading to a wide variety of possible heat-shock responses. Although molecular genetics of stress responses are highly conserved among living organisms, the individual outcome (survival, apoptosis, or necrosis) always depends on many molecular, physiological, biochemical, and environmental situations and impacts. Different organisms, different cells species, even different subcellular components and molecules may exhibit varying heat sensitivities that might be correlated with diseased conditions.[1–3] Therefore, the (patho)physiology of cellular heat stress responses is an extensive area of basic research.

We investigated the heat stress response of breast cancer cells MX1, analyzing various morphological and subcellular features requiring the application of different imaging techniques listed in Table 1. Our data supported a differentiation between continuous and discontinuous heat-induced effects on specific targets in MX1 cancer cells, which were evaluated in Table 2. The destabilization of actin cytoskeletons and the increase of cellular surface roughness were continuously enhanced by increasing temperatures. On the other hand, the adhesion and contact behavior of cells, cell shapes, and plasma membrane integrities responded in discontinuous manners. While alterations of the cell morphologies obviously initiated at a threshold temperature of approximately 45 °C, the plasma membrane integrities were not demonstrably affected until approximately 56 °C as a consequence of the selective melting behavior of biological membranes.[30] Hence, active stress response and cell necrosis should be classified as discontinuous heat-induced processes.

The most thermosensitive structure analyzed here was the actin cytoskeleton that responded to a slightly elevated temperature of 40 °C. While cell morphology, adhesion behavior, and plasma membrane integrity were not detectably affected at this stress temperature, the surface roughness increased as a consequence of cytoskeletal reorganization. In erythrocytes, actin monomers have been shown to be thermally more labile than filamentous actin.[31] Similar observations were made in microglial cells when heat-induced appearance of membrane ruffles were suggested to result from cytoskeletal reorganization involving actin as the most heat-responsive component.[32]

In our previous study, we demonstrated that mild heat stress at 40 °C leads to a transient metabolic activation of MX1 cells, resulting in enhanced cell viability.[25] At higher temperatures (45 and 50 °C), destabilization of actin filaments increased, accompanied by drastic shrinkage and rounding of cell shapes. This implies that dissolution of solid tumor tissue might be induced by heat at 45 °C or higher, but complete tumor destruction might not occur, since effective devitalization of MX1 cells was only achieved after treatment at 56 °C. In medical thermotherapy, the escape of vital cells from the tumor mass should be avoided to minimize the risk of metastases. Optimal thermotherapy protocols would therefore have to be developed to realize therapy that would define effective temperatures and temperature distributions in the target tissues without damaging adjacent healthy structures. Also, the S_a data derived from the AFM measurements in Fig. 5 denote a temperature-dependent growth of surface roughness (Fig. 6), although this phenomenon was not seen in SEM images in Fig. 2 when a pan-cellular magnification was selected. The morphological changes of cells under thermal stress generally corresponded well when the differently prepared samples imaged by different microscopic techniques were compared and did not result from preparative artefacts.

Destructive perforation of plasma membranes occurred after treatment at 56 °C,[25] as demonstrated by SEM imaging [Fig. 2(e)] and Qdot fluorescence [Fig. 4(e)] for whole cells. A detail study measured by AFM in Fig. 5(e) matched the results previously stated.

While SEM in our study was the most suitable approach for morphological and structural characterization of heat-stressed cells, the AFM provided detailed imaging of subcellular topographies in the dynamic force mode. Although SEM and AFM offer high-resolution imaging, both techniques are restricted to cell surfaces or surfaces of isolated structures, and both lack target specificity. Hence, correct interpretations of SEM or AFM imaged structures always require profound knowledge and experience. These shortcomings in principle are by-passed using fluorescence microscopy applicable to a wide variety of specific labels sensing superficial or intracellular targets.[14,15,17] The limited lateral resolution of conventional WFFM is reduced by confocal LSM, offering a greater resolution by the factor $\sqrt{2}$ if the confocal detector pinhole is smaller than the Airy disk produced by a fluorescent point.[33] The best lateral resolutions so far can be achieved by near-field microscopy, which includes AFM technologies. A combination of near-field optics and fluorescence detection has been realized with scanning near-field optical microscopy (SNOM). The SNOM technique offers high-resolution imaging of topographies and site-specific detection of fluorescence signals simultaneously, making localization of single sensor molecules possible.[34–36] Several studies have demonstrated

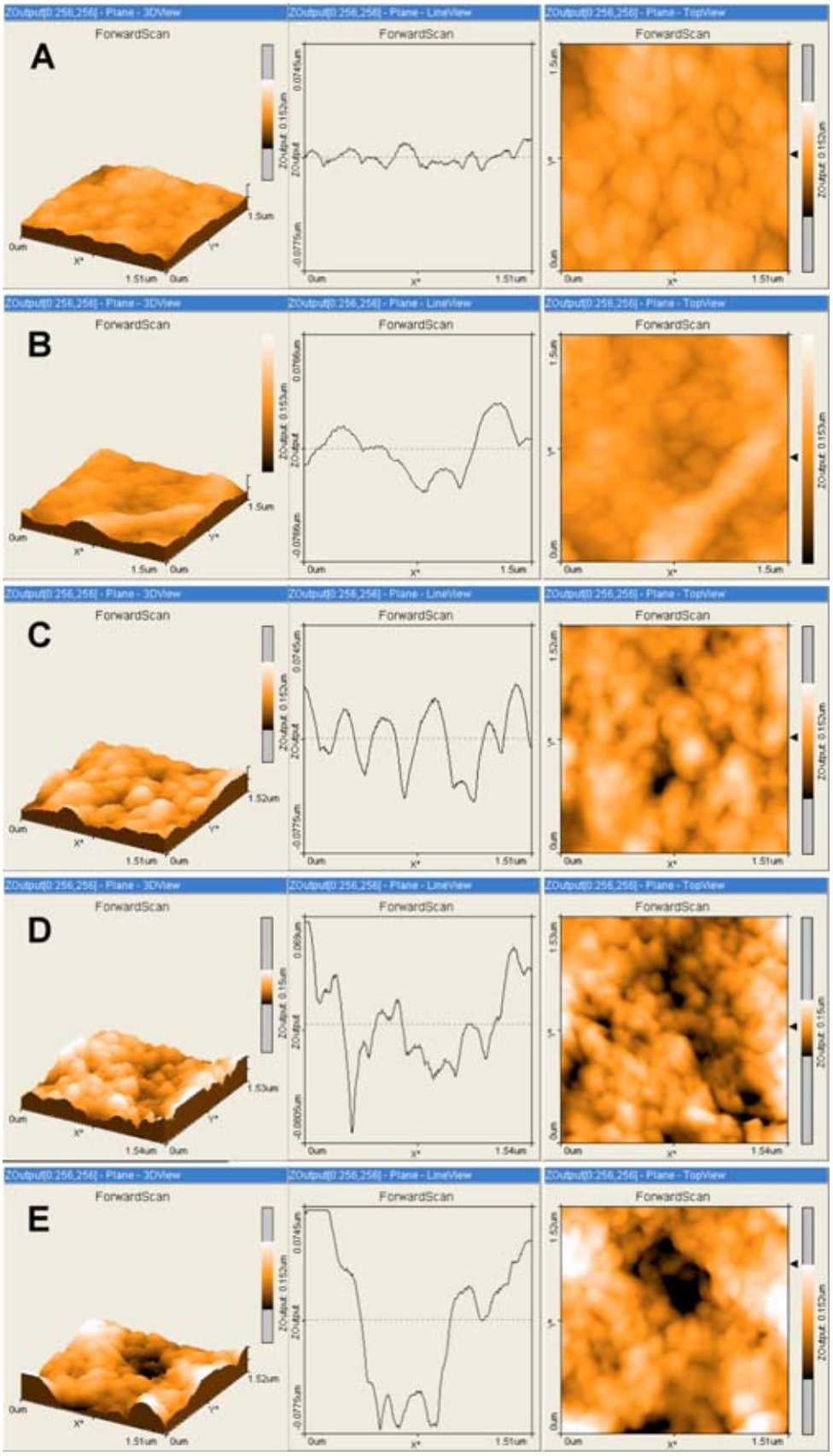

Fig. 5 AFM measurements of heat stressed cell topographies. The xy range is 1.5×1.5 μm and the dynamic Z range is 150 to 153 nm in every image. (a) Control cell, (b) cell stressed at 40 °C, (c) cell stressed at 45 °C, (d) cell stressed at 50 °C, and (e) cell stressed at 56 °C (30 min each). All panels include the 3-D profile (left) of the measured surface area, a cross section (center), and the height image (right) with the line indication (arrow head) of the cross section. Details of the measurement setup are given in Table 1.

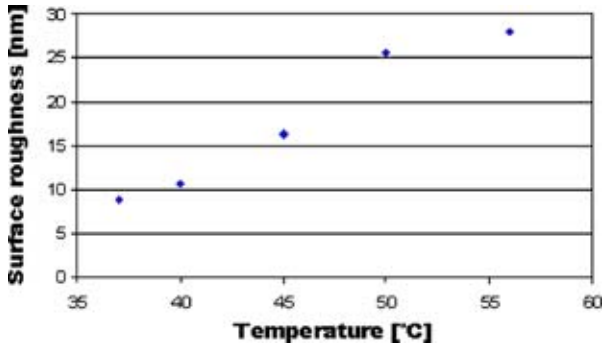

Fig. 6 Evaluations of the surface area roughness of MX1 cells treated at various heat stress conditions as indicated. The topographic measurements are shown in Fig. 5.

that supplementing AFM measurements with fluorescence images by any means is a common experimental approach in cytology when a SNOM is not available.[37–40] In SNOM investigations, Qdots should be especially useful as fluorescent labels, since they emit comparatively high signal intensities, exhibit photostability for several minutes under continuous illumination, and their broad absorption spectrum is not restricted to specific excitation sources.[41]

The long-term photostability and high emission intensity of luminescent Qdots especially support the tracking of dynamic processes in living cells, like receptor-mediated transmembrane signal transduction[42] and the lateral diffusion dynamics of glycine receptors in neuronal cells.[43]

5 Conclusion

In MX1 breast cancer cells, differential thermosensitivities of subcellular structures are detected in the heat-stress range 40 to 56 °C. Heat-induced reactions are shown to increase continuously on the fine-structural level concerning the actin cytoskeleton and the cell surface roughness resulting from molecular and supra-molecular alterations. On the other hand, the cell morphologies and the tissue architecture are observed to change discontinuously under the same heat-stress regimen. We therefore conclude that further investigations on different cell types under various heat-stress conditions will support the development of optimized thermotherapy protocols.

Table 2 Evaluation of temperature-dependent increase of stress-induced alterations in cellular target structures referred to as enhancement of effect.

Cellular target	Continuous enhancement of heat-induced effect over the temperature range 40 to 56 °C.	Discontinuous enhancement of heat-induced effect (threshold-level temperature of damage).
Retraction of cell extensions, intercellular contacts, and cell-substrate adhesion fibers.	Negative	Positive (approximately 45 °C)
Destabilization of cytoskeletal actin fibers	Positive	Negative
Decrease of plasma membrane integrity	Negative	Positive (approximately 56 °C)
Surface roughness	Positive	Negative
Morphogical changes of cell shapes	Negative	Positive (approximatel y 45 °C)

Acknowledgments

The authors wish to thank Lesley Hirst (Laser und Medizin Technologie GmbH, Berlin) for technical assistance with the SEM imaging. Parts of this work were financially supported by the Senat of Berlin (Germany) and the Deutsche Forschungsgemeinschaft (BE 1442/6-1).

References

1. S. Lindquist, "The heat shock response," *Annu. Rev. Biochem.* **55**, 1151–1191 (1986).
2. L. A. Sonna, J. Fujita, S. L. Gaffin, and C. M. Lilly, "Molecular biology of Thermoregulation," *J. Appl. Phys.* **92**, 1725–1742 (2002).
3. P. Verbeke, J. Fonager, B. F. C. Clark, and S. I. S. Rattan, "Heat response and aging: mechanisms and applications," *Cell Biol. Int.* **25**, 845–857 (2001).
4. B. Gewiese, J. Beuthan, F. Fobbe, D. Stiller, G. Müller, J. Böse-Landgraf, K. J. Wolf, and M. Deimling, "Magnetic resonance imaging-controlled laser-induced interstitial thermotherapy," *Invest. Radiol.* **29**, 345–351 (1994).
5. M. Nikfarjam and C. Christophi, "Interstitial laser thermotherapy for liver tumours," *Br. J. Surg.* **90**, 1033–1047 (2003).
6. J. van der Zee, "Heating the patient: a promising approach?" *Ann. Oncol.* **13**, 1173–1184 (2002).
7. T. Hehr, P. Wust, M. Bamberg, and W. Budach, "Current and potential role of thermotherapy for solid tumours," *Onkologie* **26**, 295–302 (2003).
8. R. Colombo, A. Salonia, L. F. Da Pozzo, R. Naspro, M. Freschi, R. Paroni, M. Pavone-Macaluso, and R. Rigatti, "Combination of intravesical chemotherapy and hyperthermia for the treatment of superficial bladder cancer: preliminary clinical experience," *Crit. Rev. Oncol. Hematol.* **47**, 127–139 (2003).
9. A. Jordan, R. Scholz, K. Maier-Hauff, M. Johannsen, P. Wust, J. Nadobny, H. Schirra, H. Schmidt, S. Deger, S. Loening, W. Lanksch, and R. Felix, "Presentation of a new magnetic field therapy system for the treatment of human solid tumors with magnetic fluid hyperthermia," *J. Magn. Magn. Mater.* **225**, 118–126 (2001).
10. M. W. Dewhirst, B. L. Viglianti, M. Lora-Michiels, M. Hanson, and P. J. Hoopes, "Basic principles of thermal dosimetry and thermal thresholds for tissue damage from hyperthermia," *Int. J. Hyperthermia* **19**, 267–294 (2003).
11. S. Takayama, J. C. Reed, and S. Homma, "Heat shock proteins as regulators of apoptosis," *Oncogene* **22**, 9041–9047 (2003).
12. J. G. Moggs and G. Orphanides, "Genomic analysis of stress response genes," *Toxicol. Lett.* **140,141**, 149–153 (2003).
13. O. Minet and J. Beuthan, "Investigating laser-induced fluorescence of metabolic changes in guinea pig livers during Nd:YAG laser irradiation," *Laser Phys. Lett.* **1**, 39-42 (2004).
14. *Fluorescent and Luminescent Probes for Biological Activity*, 2nd ed., W. T. Mason, Ed., Academic Press, San Diego, CA (1999).
15. See http://www.probes.com/handbook/.
16. E. A. Schellenberger, D. Sosnovik, R. Weissleder, and L. Josephson, "Magneto/optical annexin V, a multimodal protein," *Bioconjugate Chem.* **15**, 1062–1067 (2004).
17. See http://www.qdots.com/live/index.asp.
18. See http://www.evidenttech.com/pdf/.
19. H. Mattoussi, J. M. Mauro, E. R. Goldman, G. P. Anderson, V. C. Sundar, F. V. Mikulec, and M. G. Bawendi, "Self-assembly of CdSe–ZnS quantum dot bioconjugates using an engineered recombinant protein," *J. Am. Chem. Soc.* **122**, 12142–12150 (2000).
20. E. R. Goldman, G. P. Anderson, P. T. Tran, H. Matoussi, P. T. Charles, and J. M. Mauro, "Conjugation of luminescent quantum dots

with antibodies using an engineered adaptor protein to provide new reagent for fluoroimmunoassays," *Anal. Chem.* **74**, 841–847 (2002).
21. E. R. Goldman, E. D. Balighian, H. Mattoussi, M. K. Kuno, J. M. Mauro, P. T. Tran, and G. P. Anderson, "Avidin: a natural bridge for quantum dot-antibody conjugates," *J. Am. Chem. Soc.* **124**, 6378–6382 (2002).
22. M. E. Akerman, W. C. W. Chan, P. Laakkonen, S. N. Bhatia, and E. Ruoslahti, "Nanocrystal targeting *in vivo*," *Proc. Natl. Acad. Sci. U.S.A.* **99**, 12617–12621 (2002).
23. X. Gao, W. C. W. Chan, and S. Nie, "Quantum-dot nanocrystals for ultrasensitive biological labeling and multicolor optical encoding," *J. Biomed. Opt.* **7**(4), 532–537 (2002).
24. See http://www.qdots.com/live/upload_documents/QDV-pg2-4.pdf.
25. J. Beuthan, C. Dressler, and O. Minet, "Laser induced fluorescence detection of quantum dots redistributed in thermally stressed tumor cells," *Laser Phys.* **14**, 213–219 (2004).
26. See http://www.probes.com/media/pis/mp00354.pdf.
27. See http://www.qdots.com/live/upload_documents/90-0003.pdf.
28. easyScan DFM System, Software Reference (Version 2.0), © Nanosurf AG, Switzerland (2003).
29. V. J. Morris, A. R. Kirby, and A. P. Gunning, "Sample roughness," Chap. 3.5.4. in *AtomicForce Microscopy for Biologists*, pp. 61–63, Imperial College Press, London (2001).
30. T. Heimburg, "Mechanical aspects of membrane thermodynamics. Estimation of the mechanical properties of lipid membranes close the chain melting transition from calorimetry," *Biochim. Biophys. Acta* **1415**, 147–162 (1998).
31. W. T. Coakley, "Hyperthermia effects on the cytoskeleton and on cell morphology," *Symp. Soc. Exp. Biol.* **41**, 187–211 (1987).
32. F. Macouillard-Poulletier de Gannes, M. Merle, P. Canioni, and P. J. Voison, "Metabolic and cellular characterization of immortalized human microglial cells under heat stress," *Neurochem. Int.* **33**, 61–73 (1998).
33. S. Inoué, "Foundations of confocal scanned imaging in light microscopy," Chap. 1 in *Handbook of Biological Confocal Microscopy*, 2nd ed., J. B. Pawley, Ed., pp. 1–17, Plenum Press, New York (1995).
34. F. de Lange, A. Cambi, R. Huijbens, B. de Bakker, W. Rensen, M. Garcia-Parajo, N. van Hulst, and C. G. Figdor, "Cell biology beyond the diffraction limit: near-field scanning optical microscopy," *J. Cell. Sci.* **114**, 4153–4160 (2001).
35. S. Rieti, V. Manni, A. Lisi, L. Giuliani, D. Sacco, E. D'Emilia, A. Cricenti, R. Generosi, M. Luce, and S. Grimaldi, "SNOM and AFM microscopi techniques to study the effect of non-ionizing radiation on the morphological and biochemical properties of human keratinocytes cell line (HaCaT)," *J. Microsc.* **213**, 20–28 (2003).
36. J. K. H. Hoerber and M. J. Miles, "Scanning probe evolution in biology," *Science* **302**, 1002–1005 (2003).
37. M. Micic, D. Hu, Y. D. Suh, G. Newton, M. Romine, and H. P. Lu, "Correlated atomic force microscopy and fluorescence lifetime imaging of live bacterial cells," *Colloids Surf., B* **34**, 205–212 (2004).
38. G. de Stasio, B. H. Frazer, M. Girasole, L. M. Wiese, E. K. Krasnowska, G. Greco, A. Serafino, and T. Parasassi, "Imaging the cell surface: argon sputtering to expose inner cell structures," *Microsc. Res. Tech.* **63**, 115–121 (2004).
39. J. A. Dvorak, "The application of atomic force microscopy to the study of living vertebrate cells in culture," *Methods* **29**, 86–96 (2003).
40. C. Rotsch and M. Rademacher, "Drug-induced changes of cytoskeletal structures and mechanisms in fibroblasts: an atomic force microscopy study," *Biophys. J.* **78**, 520–535 (2000).
41. X. Wu, H. Liu, J. Liu, K. N. Haley, J. A. Treadway, J. P. Larson, N. Ge, F. Peale, and M. P. Bruchez, "Immunofluorescent labeling of cancer marker Her2 and other cellular targets with semiconductor quantum dots," *Nat. Biotechnol.* **21**, 41–46 (2003).
42. D. S. Lidke, P. Nagy P, R. Heintzmann, D. J. Arndt-Jovin, J. N. Post, H. E. Grecco, E. A. Jares-Erijman, and T. M. Jovin, "Quantum dot ligands provide new insights into erbB/Her receptor-mediated signal transduction," *Nat. Biotechnol.* **22**, 198–203 (2004).
43. M. Dahan, S. Lévi, C. Luccardini, P. Rostaing, B. Riveau, and A. Triller, "Diffusion dynamics of glicine receptors revealed by single-quantum dot tracking," *Science* **302**, 442–445 (2003).